JASMAC
Conference of the Japan Society of Microgravity Appllication
JSMA

OS3-2

長時間微小重力燃焼実験における NOMEX の燃え拡がり挙動

Flame Spread Behavior of NOMEX Sheets in Long-Duration Microgravity Experiments

高橋周平 [1]，小林芳成 [1]，菊池政雄 [2]，藤田修 [3]
Shuhei TAKAHASHI[1], Yoshinari KOBAYASHI[1], Masao KIKUCHI[2] and Osamu FUJITA[3]
[1] 岐阜大学，Gifu University
[2] 宇宙航空研究開発機構，Japan Aerospace Exploration Agency
[3] 北海道大学，Hokkaido University

* Correspondence: takahashi.shuhei.s0@f.gifu-u.ac.jp

Abstract: Long-duration combustion experiments of NOMEX HT90-40, a high-oxygen-index (OI = 30) charring material, were conducted aboard the International Space Station using the Solid Combustion Experiment Module (SCEM) under both opposed-flow and concurrent-flow conditions. The study aimed to evaluate the applicability of a previously proposed scaling model for predicting flammability limits of solid materials in microgravity. Under opposed-flow conditions, the model quantitatively reproduced the limiting conditions for two-dimensional flame spread. At velocities below the predicted limiting curve, the flame transitioned to a robust three-dimensional structure, reducing the preheat-zone length and thereby lowering radiative heat losses—behavior also observed for filter paper. In contrast, under concurrent-flow conditions, extinction occurred even at oxygen concentrations that supported steady flame spread under opposed-flow conditions. This phenomenon is attributed to oxygen consumption in the upstream char region, reducing oxygen availability in the pyrolysis zone. These findings establish quantitative flammability thresholds for high-OI charring materials in microgravity, providing a robust basis for refining fire-safety standards in space habitats. They also underscore the importance of further investigations into ignition-energy history, flow-field effects, and oxygen-distribution non-uniformity under varied environmental conditions.

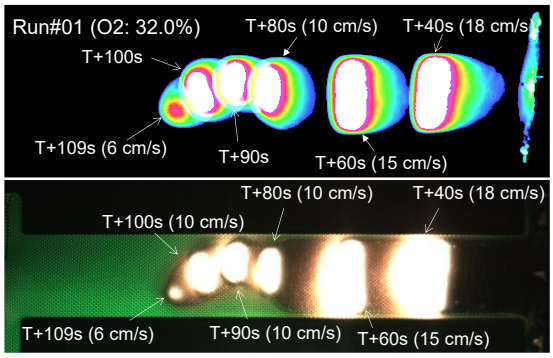

Keywords: Flame spread, Flammability limit, Charring-materials, Microgravity

1. Introduction

Ensuring fire safety is one of the critical challenges in long-duration human space activities[1)]. In recent years, the utilization of space by the private sector has been expanding, creating a growing need for methods capable of evaluating the flammability of solid materials across a broader range of gravity levels and atmospheric environments. Under the FLARE project, led by the Japan Aerospace Exploration Agency (JAXA), a new fire safety standard for solid materials has been proposed[2)]. As part of this effort, long-duration microgravity experiments using flat-plate specimens have been conducted since 2022 aboard the ISS/Kibo module, employing the Solid Combustion Experiment Module (SCEM). Previous studies in this series have included combustion tests of filter paper[3, 4)] and polymethyl methacrylate[5)] (PMMA), both widely used as

standard specimens from earlier research. In 2024, combustion tests began on NOMEX HT90-40, a meta-aramid fabric with flame-retardant properties. NOMEX, which is also used in space suits, exhibits a high oxygen index (OI = 30) and is classified as a charring material, leaving solid residue after burning. This paper presents the characteristic burning behaviors of NOMEX specimens observed under varying conditions of ambient oxygen concentration, ambient pressure, and external flow velocity.

2. Model for predicting flammability limits

In the scaling analysis, the limiting oxygen concentration (LOC) for a two-dimensional flame under opposed-flow conditions (Fig. 1) was determined by establishing a thermal balance equation[6] (Eq. 1).

$$V_f \rho_s c_s \tau (T_v - T_\infty) + \varepsilon(1-\alpha_{abs})\sigma\left(T_v^{\,4} - T_\infty^{\,4}\right)L_g = \left(1 - \frac{1}{Da}\right)\lambda_g \frac{(T_f - T_v)}{L_g} L_g \qquad (1)$$

In this equation, V_f denotes the flame-spread velocity, Da is the Damkohler number, and ρ_s, c_s, τ, and T_v are the density, specific heat, thickness, and pyrolysis temperature of the sample, respectively. λ_g is the thermal conductivity of the gas phase (evaluated at T_v), and L_g is the preheat-zone length. In addition, σ and ε represent the Stefan-Boltzmann constant and the emissivity of the sample surface, respectively. By non-dimensionalizing Eq. 1 using the flame-spread velocity $V_{f,th}$ in the so-called thermal regime, the following non-dimensional equation (Eq. 2) is obtained.

$$\eta + R_{rad} + \frac{1}{Da} = 1 \qquad where \quad \eta = \frac{V_f}{V_{f,th}} \qquad \left(V_{f,th} = \frac{\lambda_g}{\rho_s c_s \tau}\frac{T_f - T_v}{T_v - T_\infty}\right) \qquad (2)$$

The preheat-zone length L_g in Eq. 1 is expressed, based on results from orbital experiments with filter paper[4], as $L_g \sim (\mathrm{Pr}\cdot x_d \cdot \alpha_g / V_g)^{0.5}$. Using this relation, R_{rad} and Da in Eq. 2 can be written as follows:

$$R_{rad} = B_2{}' \cdot \frac{\varepsilon(1-a_{abs})\sigma(T_v^4 - T_\infty^4)}{\rho_g c_g (T_f - T_v)} \sqrt{\frac{Pr x_d}{V_g \alpha_g}} \qquad (3)$$

$$Da = Pr \frac{x_d}{V_g} \rho_g Y_O A^* \, exp(-E^*/RT_f) \qquad (4)$$

Here, the parameters A' and E' in Da are calculated from the oxygen index[7] (OI) and the high-velocity oxygen index[8] (HOI). The experimental constant B_2' in R_{rad} was set to $B_2' = 1.08$ based on orbital experimental results with filter paper[4]. The physical properties used for the predictions are summarized in Table 1. The predicted limiting curve is then compared with flame-spread experimental results obtained in orbit.

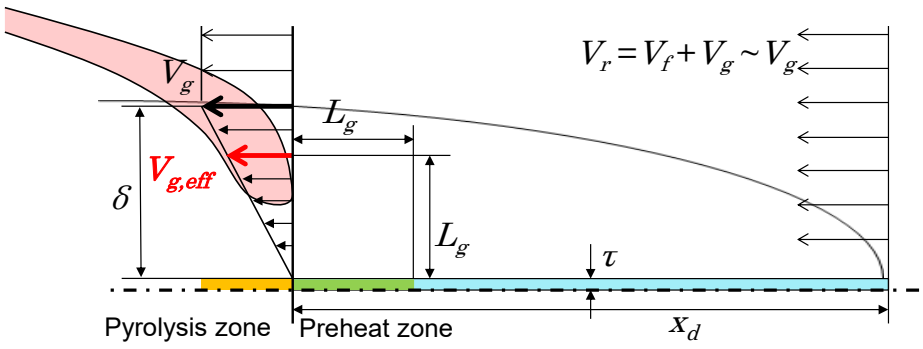

Figure 1. Schematic of two-dimensional flame spread over a thin solid material under opposed-flow conditions.

Table 1. Properties of NOMEX

	Chemical formula	Area density [g/m²]	Thickness [mm]	OI	HOI_{800}	HOI_{1000}	T_v [K]	Δh [kJ/g]
NOMEX HT90-40	$C_{14}H_{10}O_2N_2$	244	0.30	30.03	30.59	30.83	745	25.53

OI: oxygen index; HOI: high-velocity oxygen index; T_v: pyrolysis temperature; Δh: heat of combustion

3. Experimental setup

The experiments were conducted using the Solid Combustion Experiment Module[3, 4] (SCEM) installed in the Kibo module of the International Space Station (ISS). An overview of SCEM is shown in Fig. 2. SCEM is a closed-circuit wind tunnel with an internal volume of 35 liters. A flat sample (2 cm wide, 13 cm long) mounted on a sample card is placed in the test section, enabling experiments under both opposed-flow and concurrent-flow conditions by varying the ignition position. Ignition was achieved by electrically heating a Kanthal wire in contact with the sample edge. In the experimental results, time is represented as follows: T+0s corresponds to the start of recording, T+5 s marks the beginning of heating the ignition wire, and the heating duration was set to 10 seconds.

The oxygen concentration and ambient flow velocity inside SCEM can be controlled in the ranges 0–45% and 0–30 cm/s, respectively, while the atmospheric pressure can be adjusted from 0 to 101.3 kPa. Flame-spread behavior was recorded by three visible-light cameras (frame rate: 20 fps) positioned perpendicularly, diagonally, and horizontally to the sample. The sample-surface temperature was measured using an infrared camera (wavelength range: 7–13 μm, frame rate: 30 fps) with a measurable range of 243–803 K.

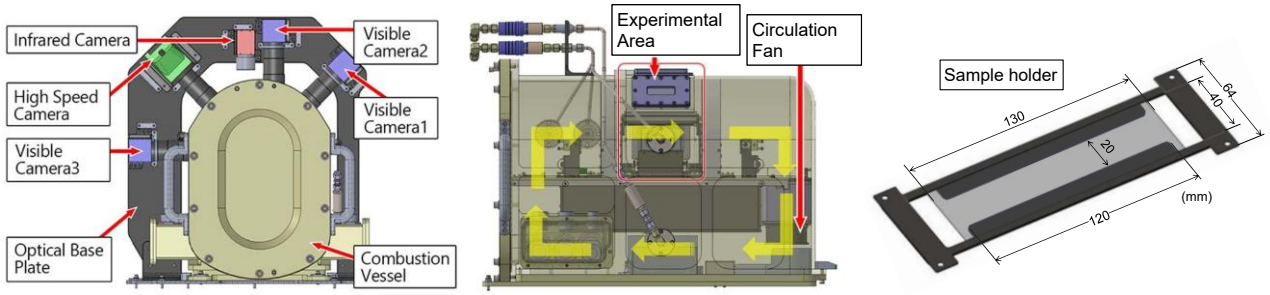

Figure 2. Solid Combustion Experiment Module (SCEM) on the ISS/Kibo module

4. Results and discussion

Long-duration combustion experiments of NOMEX were conducted under both opposed-flow and concurrent-flow conditions at atmospheric pressure (101.3 kPa), with eight tests performed for each condition. The flammability map obtained under opposed-flow conditions is shown in Fig. 3, together with the limiting

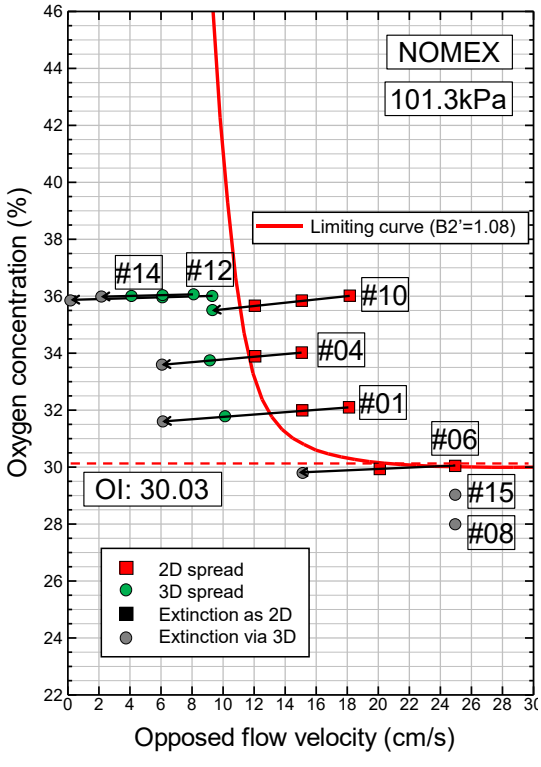

Figure 3. Flammability map of NOMEX under opposed flow conditions.

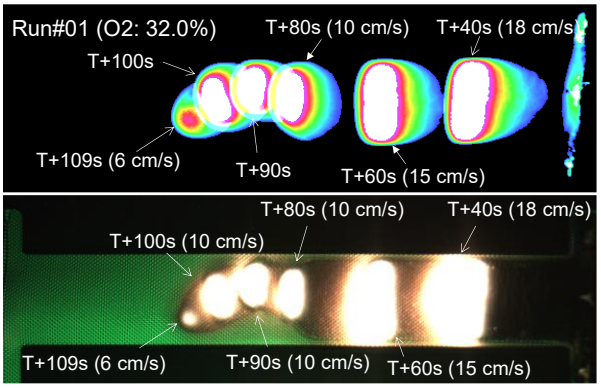

Figure 4. Flame spread behavior in Run #01. Opposed-flow velocity (Vg) decreases as follows: 18 cm/s [T+0s] → 15 cm/s [T+40s] → 10 cm/s [T+70s] → 6 cm/s [T+100s]

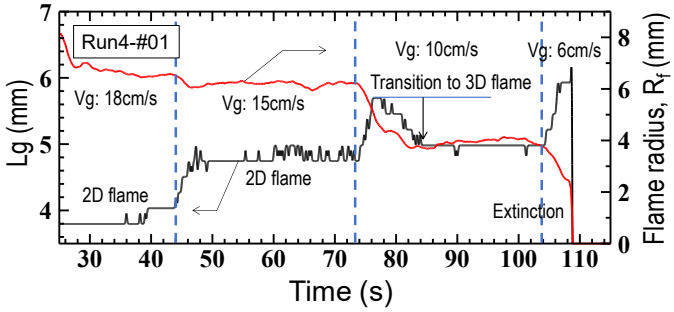

Figure 5. Time histories of the preheat-zone length (L_g) and flame radius (R_f) in Run #01.

curve calculated from Eqs. 1–4 using the physical properties listed in Table 1. Most of the samples were tested under conditions where the flow velocity was varied stepwise. In the figure, squares indicate cases where a two-dimensional flame was observed, while circles denote cases where a three-dimensional flame was observed. It is evident that two-dimensional flames appeared within the predicted limiting curve. Beyond this curve, as the opposed-flow velocity decreased, the flame transitioned from a two-dimensional to a three-dimensional structure, and further reduction in velocity led to extinction. This behavior was also observed in tests using filter paper[3].

The change in flame structure with decreasing flow velocity is illustrated in Fig. 4 (Run #01). When the opposed-flow velocity reached 10 cm/s, the initially two-dimensional flame became rounded, and at 6 cm/s it was extinguished. This transition can be explained by differences in preheat-zone length (L_g) between two-dimensional and three-dimensional flames. Equations 5 and 6 describe L_g for two-dimensional and three-dimensional flames, respectively.

$$L_g \sim \sqrt{\frac{Pr x_d \alpha_g}{V_g}} \qquad \text{(for two-dimensional flame)} \qquad (5)$$

$$L_g \sim \frac{2R_f}{2 + 0.6Re^{\frac{1}{2}}Pr^{\frac{1}{3}}} \propto R_f \quad where\ Re = \frac{2R_f V_g}{\nu} \sim O(10) \qquad \text{(for three-dimensional flame)} \qquad (6)$$

For a two-dimensional flame, L_g increases rapidly as the opposed-flow velocity decreases. However, when the flame assumes a three-dimensional shape, L_g becomes approximately proportional to the flame radius, allowing the flame to shorten L_g by reducing its radius. This reduction in L_g is considered to reduce radiative heat losses. Figure 5 presents the time histories of L_g and the flame radius, R_f, for Run #01. The flame radius is defined as the radius of a circle having the same area as the observed flame. Initially, L_g increases stepwise with decreasing opposed-flow velocity. When the velocity reaches 10 cm/s, L_g first rises to 5.7 mm, corresponding to that velocity, but after the flame transitions to a three-dimensional structure, L_g decreases to 5.0 mm, thereby reducing radiative losses.

The flammability map for concurrent-flow conditions is shown in Fig. 6. In this case, extinction was observed even at oxygen concentrations where flame spread occurred under opposed-flow conditions,

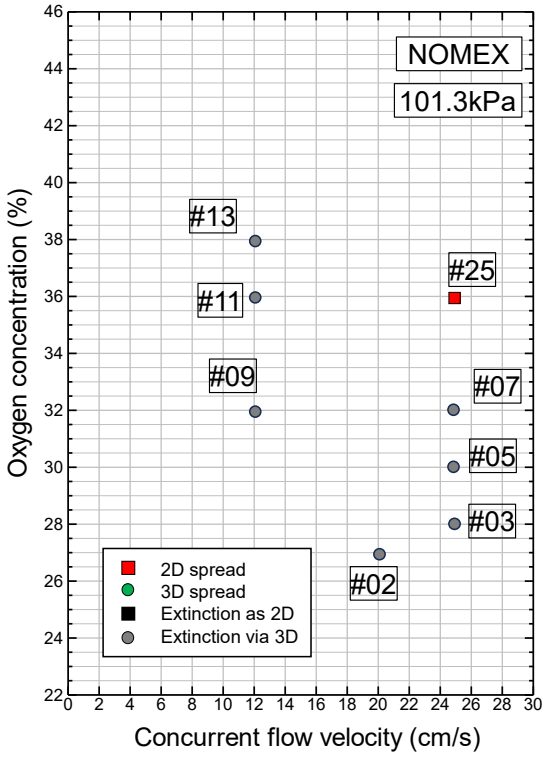

Figure 6. Flammability map of NOMEX under concurrent flow conditions.

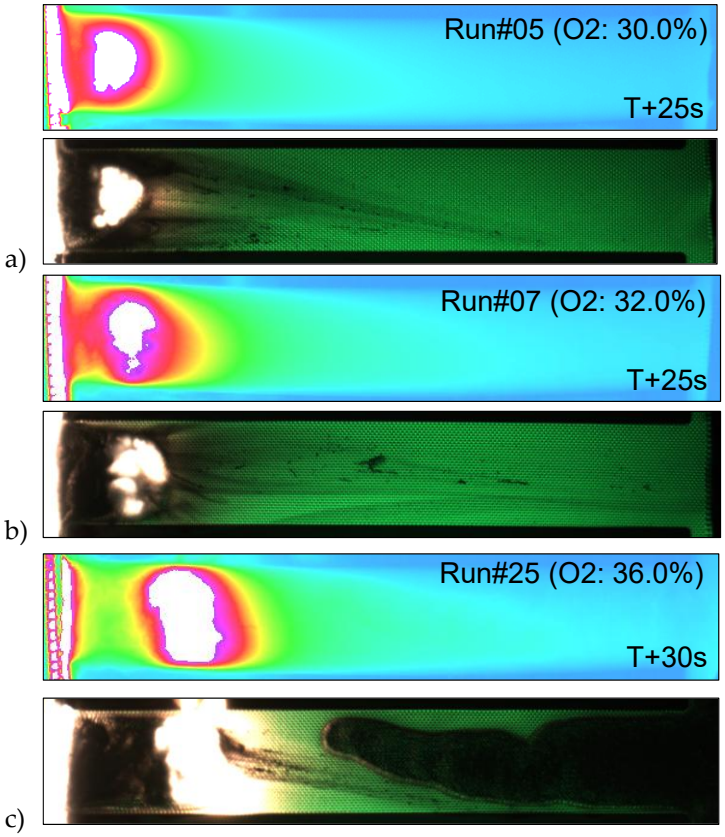

Figure 7. Flame spread behavior in a) Run #05, b) Run #07, and c) Run #25.

yielding the unexpected result that burning was less sustainable under concurrent flow. The ignition power and heating duration for the Kanthal wire were identical to those in the opposed-flow experiments. Infrared images from Run #05 and Run #07 (Figs. 7a, b) show that, immediately after ignition, the flame assumed a rounded shape even at relatively high velocities and was rapidly extinguished. Furthermore, in Run #25, where steady flame spread was achieved, the shape of the hot charred edge fluctuated significantly over time (see Fig. 7c).

These findings indicate that concurrent-flow conditions are not necessarily more conservative than opposed-flow conditions. Although not shown here, similar phenomena were also observed at a reduced ambient pressure of 56.5 kPa. On the other hand, upward flame-spread tests conducted on the ground have reported sustained combustion at an oxygen concentration of 26%[9], a result also confirmed in our previous experiments. This suggests that flame spread under concurrent-flow conditions is strongly influenced by the ignition energy history, differences in the surrounding flow field, and, as discussed above, oxygen-concentration non-uniformity.

5. Conclusions

Long-duration combustion experiments of NOMEX were conducted under both opposed-flow and concurrent-flow conditions, yielding the following key findings:

1. The previously proposed model equations quantitatively reproduced the limiting conditions for two-dimensional flame spread of NOMEX under opposed-flow conditions.
2. Under opposed-flow conditions at velocities below the limiting curve, the flame transitioned to a three-dimensional structure—similar to the behavior observed for filter paper—resulting in a robust flame. This transition effectively reduced the preheat-zone length compared to a two-dimensional flame, thereby reducing radiative heat losses.
3. Under concurrent-flow conditions, extinction occurred even at oxygen concentrations that supported steady flame spread in opposed-flow tests. This phenomenon is likely caused by oxygen consumption due to oxidation reactions in the upstream char region, leading to reduced oxygen availability in the pyrolysis zone.

These findings provide new insight into the flammability behavior of high-OI charring materials in microgravity and demonstrate that concurrent-flow conditions are not inherently more conservative than opposed-flow conditions. By establishing quantitative limits for high-OI charring materials in microgravity, this study offers a robust foundation for revising fire-safety standards for space habitats. These findings also underscore the importance of future investigations into ignition-energy history, flow-field effects, and oxygen distribution under diverse environmental conditions.

Acknowledgments

This study was carried out as part of the FLARE project, supported by the Japan Aerospace Exploration Agency (JAXA) under the third phase of JEM/ISS utilization program, “Evaluating the Impact of Gravity on the Combustion Phenomena of Solid Materials for Enhanced Fire Safety.” We gratefully acknowledge the valuable contributions and insightful suggestions provided by all members of the FLARE project team.

Conflicts of Interest

The authors declare no conflict of interest.

References

1) U. Rojas-Alva, G. Jomaas, A historical overview of experimental solid combustion research in microgravity, Acta Astronautica **194** (2022) 363-375, DOI: 10.1016/j.actaastro.2022.01.037.
2) O. Fujita, Solid combustion research in microgravity as a base of fire safety in space, Proc. Combust. Inst. **35** (2015) 2487–2502, DOI: 10.1016/j.proci.2014.08.010.
3) S. Takahashi, H. Torikai, Y. Kobayashi, M. Kikuchi, O. Fujita, Flame Spread Behavior Over a Filter Paper Near Extinction Limit Under Microgravity on the ISS/Kibo, Fire Technology **60** (2023) 313-334, DOI: 10.1007/s10694-023-01507-3.
4) S. Takahashi, H. Torikai, Y. Kobayashi, M. Kikuchi, O. Fujita, Quantitative prediction of the flammability limits of filter paper in microgravity conditions, Proc. Combust. Inst. **40** (2024) 105200, DOI: 10.1016/j.proci.2024.105200.

5) Y. Kurauchi, K. Hanamoto, Y. Kobayashi, S. Takahashi, Proc. 62nd Symp. (Japanese) on Combust. (2024), A123 (in Japanese).
6) S. Takahashi, M. A. F. bin Borhan, K. Terashima, A. Hosogai, Y. Kobayashi, Flammability limit of thin flame retardant materials in microgravity environments, Proc. Combust. Inst. **37** (2019) 4257-4265, DOI: 10.1016/j.proci.2018.06.102.
7) ISO 4589-2:2017: Plastics, Determination of burning behaviour by oxygen index, Part 2: Ambient-temperature test, https://www.iso.org/standard/60786.html.
8) ISO 4589-4:2021: Plastics, Determination of burning behaviour by oxygen index, Part 4: High gas velocity test, https://www.iso.org/standard/75215.html.
9) A. F. Osorio, C. Fernandez-Pello, D. L. Urban, G. A. Ruff, Limiting conditions for flame spread in fire resistant fabrics, Proc. Combust. Inst. **34** (2013) 2691-2697, DOI: 10.1016/j.proci.2012.07.053.